Catalysis Today 172 (2011) 143–151

Contents lists available at ScienceDirect

Catalysis Today

journal homepage: www.elsevier.com/locate/cattod

Ni-Co-Mg-Al catalysts for hydrogen and carbonaceous nanomaterials production by CCVD of methane

N. Latorre, F. Cazaña, V. Martínez-Hansen, C. Royo, E. Romeo, A. Monzón*

Institute of Nanoscience of Aragon, Department of Chemical and Environmental Engineering, University of Zaragoza, 50009 Zaragoza, Spain

ARTICLE INFO

Article history:
Received 30 November 2010
Received in revised form 14 February 2011
Accepted 14 February 2011
Available online 1 April 2011

Keywords:
Hydrogen production
CNT growth
Ni-Co catalysts
Nanocarbonaceous materials
Methane decomposition
Kinetic modeling
CCVD
Catalyst deactivation

ABSTRACT

This paper reports the characterization and catalytic results of a bimetallic Ni-Co/Mg-Al catalyst during the methane decomposition reaction for the co-production of H_2 and nanocarbonaceous materials (e.g. carbon nanotubes-CNTs). The catalyst has been characterized before and after reaction with the aim of observing the changes in its structure and also the type of nanocarbonaceous materials formed. The influence on CNT growth rate, of the temperature during the calcination and reaction stages has been studied. The activity, stability and selectivity to the production of hydrogen and carbon nanotubes greatly depend on the catalyst composition and on the activation and reaction conditions used. The bimetallic Ni-Co/Mg-Al catalyst, prepared by controlled coprecipitation, shows higher stability that the monometallic catalysts Ni/Mg-Al and Co/Mg-Al. TEM and TPO observations indicate that the type of nanocarbonaceous material obtained when the catalyst does not suffer deactivation, corresponds to multi-wall carbon nanotubes (MWNT), with average diameter of ca. 20 nm.

The kinetic results of CNT formation, obtained in a thermobalance, were evaluated using a Phenomenological Kinetic Model that includes the main relevant steps involved in CNT growth by catalytic decomposition of hydrocarbons (CCVD): (i) hydrocarbon decomposition at the gas side; (ii) carburization of the metallic nanoparticle surface; (iii) atom carbon diffusion (bulk and/or surface) (iv) nucleation and CNT growth; and finally (v) growth termination by catalyst deactivation or by the effect of steric hindrance of the CNTs formed. In this paper we have applied the Phenomenological Kinetic Model to study the influence of the calcination and reaction temperature. The obtained values for the kinetic parameters have realistic physical meaning in good agreement with the mechanism considered during the formation and growth of carbon nanotubes.

1. Introduction

The attractive possibilities of using the outstanding properties of carbon nanotubes (CNT) and other new carbonaceous nanomaterials like carbon nanofibers (CNF) in a broad range of new applications, is motivating substantial research effort in practically all fields of Nanoscience and Nanotechnology [1–3].

Catalytic chemical vapor deposition (CCVD) has become probably the main technique for the synthesis of carbon nanotubes, due to its ease of scale significantly reducing production costs [4]. The role of the catalyst is crucial for obtaining a considerable volume of production and high quality nanotube formation. Fe, Co, and Ni, as well as their alloys are the active metals usually utilized in the composition of the catalyst used in this process [5].

If methane is used as the carbon source, hydrogen is obtained as a co-product. Hydrogen is a clean fuel that emits no CO_2 when burned or used in H_2–O_2 fuel cells, can be stored as a liquid or gas, and is distributed via pipelines [6]. Therefore, a growing demand is forecast in most industrial and energy sectors, including petroleum refining where the increasing need to process heavy and high-sulphur content crude-oil is accompanied by the lowering of hydrogen co-product in the catalytic reforming process. At present, catalytic methane decomposition is not used industrially since it is not yet economically competitive with the well-developed methane steam reforming process. However, the currently increasing demand for CO-free hydrogen, a continuous catalytic process for methane decomposition is becoming more interesting. High methane conversion and utilization of the produced carbonaceous materials are essential factors for process economics [7].

Our research group has worked on the development of Ni and Co based catalysts, using hydrotalcite-like compounds as precursors, for application in the CCVD process, optimizing the catalyst composition and the addition of promoters [8–16]. Ni based catalysts show high productivity during the CCVD reaction [8–11,14]. However, the selectivity to carbon nanotubes is low (especially if they are modified by addition of Cu), producing mainly CNFs of

* Corresponding author. Tel.: +34 976 761157; fax: +34 976 761879.
E-mail address: amonzon@unizar.es (A. Monzón).

0920-5861/$ – see front matter © 2011 Elsevier B.V. All rights reserved.
doi:10.1016/j.cattod.2011.02.038

different morphologies [9,10]. On the other hand, Co based catalysts (type Co-Mg-Al) suffer high deactivation during the reaction [12,13]. These catalysts have to be calcined at low temperatures (400 °C) to achieve their reduction and consequently activity [12]. However, at this calcination temperature, solids with low particle diameters are formed, improving their selectivity to produce carbon nanotubes.

The goal of this work is to develop materials based on these two metals, Ni and Co, trying to achieve catalysts with good stability and selectivity to CNTs. In addition to the composition of the catalyst, operating conditions strongly determine the selectivity and the stability of the catalyst. Thus, the influence of the calcination temperature and the operating conditions on carbon production and carbon formation rate has been studied. In order to get a more deep insight of the mechanism involved in this process, a *Phenomenological Kinetic Model* has been applied to fit our experimental data [15,16]. This model takes into account the influence of all the phenomena involved in the carbon filament growth, allowing the influence of each stage to be discriminated.

2. Experimental

The bimetallic Ni-Co/Mg-Al catalyst, with nominal composition $(NiO)_{0.5}(CoO)_{0.5}(MgO)_{0.5}(MgAl_2O_4)_{0.5,}$ was prepared by controlled coprecipitation of the metallic nitrate mixture (Ni, Co, Mg and Al) with Na_2CO_3/NaOH, at constant pH (10.2 ± 0.2) and temperature (60 °C) [9–12,14,17]. The corresponding mixed oxide was obtained by calcination of the dried hydrated precursor in N_2 at 400 and 800 °C for 11 h. This catalyst was compared with the monometallic catalysts Ni/Mg-Al and Co/Mg-Al, that have the following nominal compositions: $(NiO)_{0.5}(MgO)_{0.5}(MgAl_2O_4)_{0.5,}$ and $(CoO)_{0.5}(MgO)_{0.5}(MgAl_2O_4)_{0.5}$, respectively. These catalysts where prepared using the same procedure as Ni-Co/Mg-Al catalyst.

The catalysts were characterized by several techniques. The metallic content was determined by atomic absorption (AA) with a spectrophotometer SpectrAA 110 (Varian Inc.). The X-ray diffraction (XRD) patterns were recorded within the range of 5–85° (2θ) in Rigaku/Max Cu rotatory anode equipment.

Nitrogen adsorption–desorption isotherms of the samples were measured at 77 K using a porosity analyzer (TriStar 3000, Micromeritics Instrument Corp.). The samples were outgassed with a heating rate of 10 °C/min until 90 °C and maintained for 1 h, and then the temperature was raised till 200 °C and maintained for 8 h. BET specific surface areas were measured from the adsorption branches in the relative pressure range of 0.05–0.25. The area and volume of micropores were estimated using *t-method* and the pore size distributions were calculated using the Barrett–Joyner–Halenda (BJH) model from the adsorption branches.

The reaction was carried out at atmospheric pressure in a thermobalance (CI Electronics Ltd., UK, model MK2) operated as a differential reactor, equipped with mass flow and temperature controllers. This experimental system allows continuous recording of the sample weight and temperature during reaction. Catalyst reduction was carried out *in situ* using a 40% H_2/60% N_2 mixture. The reaction conditions were as follows: sample weight: 100 mg; temperature range: 550–625 °C; total flow-rate: 750 N ml/min.; feed composition: 5%CH_4/95%N_2.

After reaction, the catalyst, as well as the carbon obtained, was characterized by transmission electron microscopy (TEM), X-Ray Diffraction (XRD), and temperature programmed oxidation (TPO).

TEM micrographs images were recorded in a JEOL-2000 FXII microscope, operated at 150 kV, so that the irradiation damages were limited. Samples for TEM were prepared by making sonicated suspensions in ethanol and depositing a few droplets of the suspensions onto regular copper microgrids coated with a lacey carbon film.

TPO and TPR measurements were carried out in a ChemBET PULSAR instrument (Quantachrome Instruments). The TPO conditions were: feed composition: 10% O_2/90% N_2, gas flow-rate: 20 ml/min, sample weight: 20 mg, and heating rate was 10 °C/min. The TPR conditions were: feed composition: 5% H_2/95% N_2, gas flow-rate: 100 ml/min, sample weight: 200 mg, and heating rate was 5 °C/min.

3. Results and discussion

3.1. Catalyst characterization

The results of atomic absorption indicate that the actual composition differs little from the nominal composition, confirming the good reproducibility of the method of preparation [8–17]. Thus, from the composition measured by atomic absorption, the corresponding formulas of the three catalysts are: Ni/Mg-Al: $(NiO)_{1,23}(MgO)_{0,59}(MgAl_2O_4)_{0,41}$; Co/Mg-Al: $(CoO)_{0,95}(MgO)_{0,63}(MgAl_2O_4)_{0,37}$ and Ni-Co/Mg-Al: $(NiO)_{0,44}(CoO)_{0,49}(MgO)_{0,64}(MgAl_2O4)_{0,36}$. These Mg/Al ratios in the three catalysts are 1.2, 1.3 and 1.4 respectively. These values are more than twice times the ration Mg/Al in the $MgAl_2O_4$ phase, indicating that the catalyst support is a mixture of MgO and $MgAl_2O_4$.

Fig. 1a and b shows the XRD patterns of the catalysts before and after reaction. In Fig. 1a are presented XRD patterns after calcination of the three catalysts. In all the cases are detected the presence of oxide (i.e. CoO, NiO and MgO) and spinel phases, in accordance with the AA results. As was expected, the lower the calcination temperature is, the lower the crystallinity of the solid. At 800 °C the peaks are sharper and the size of the crystals is higher. After calcination at 800 °C, the peaks corresponding to MgO and to $MgAl_2O_4$ and possibly $CoAl_2O_4$ spinel phases can be clearly observed. However, it is difficult to determine what of the dispositive cations (Mg^{+2}, Ni^{+2} or Co^{+2}) are present in the inner part of the crystalline structure, due to the fact that the angles and related intensities of the diffraction bands for the $CoAl_2O_4$ and $MgAl_2O_4$ spinels are quite similar. Besides, it must be considered that the small size of the particles of the metallic oxides of NiO and CoO averts the detection by XRD. However, this small size of the NiO and CoO nanoparticles is an advantage for the selective production of CNTs, whose diameter strongly depends on the metallic particle size from which they grow.

The peaks of the XRD obtained for the catalysts calcined at 400 °C are much wider and less defined, corresponding to a less crystalline structure, and the identification of the peaks is very difficult in the case of this type of diffractogram. Therefore, it cannot be assured if the structure formed corresponds to the metallic oxides dispersed on a spinel phase or if the spinel phase has not crystallized and the solid structure corresponds to a mixture of metallic oxides. After reaction, the XRD patterns, Fig. 1b, show the presence of the following phases: metallic NiO and CoO, formed during the reduction process; graphitic carbon, MgO and $MgAl_2O_4$. Therefore, after reduction stage, the catalyst has the metallic nanoparticles of Ni and/or Co dispersed over the surface of MgO mixed with $MgAl_2O_4$, which are acting as support.

Fig. 2 shows the N_2 adsorption/desorption isotherms for the Ni-Co/Mg-Al catalyst calcined at 400 °C and 800 °C. These isotherms correspond to isotherms type IV typical of mesoporous materials. However, the hysteresis loop of the sample calcined at 400 °C is of the type H2 according to the IUPAC classification [18]. This type of hysteresis is associated to disordered materials with a non-well defined shape and pore size distribution [19], in accordance with the XRD results. The sample calcined at 800 °C shows

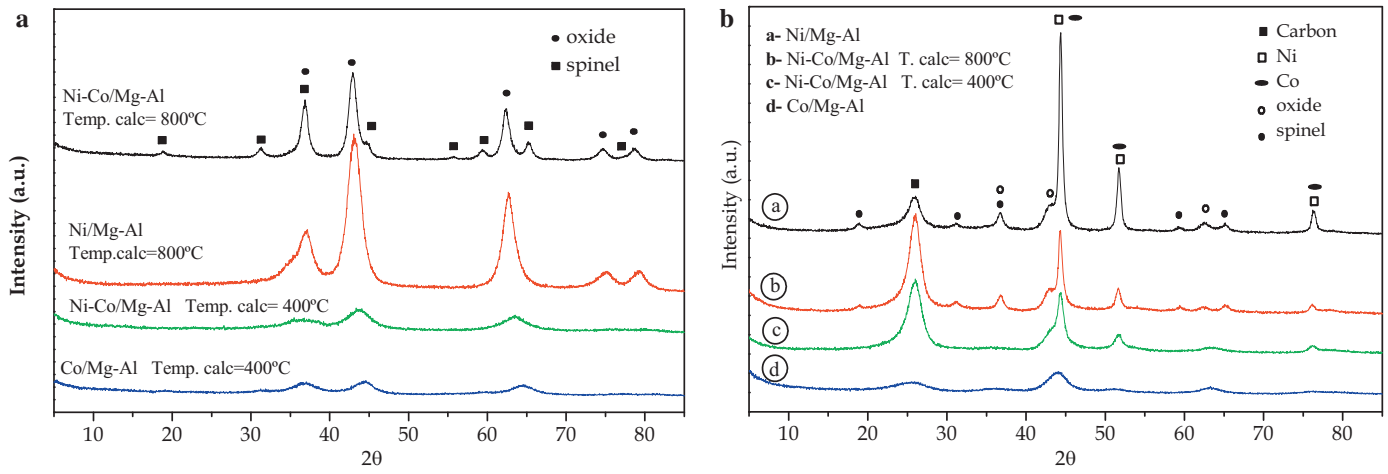

Fig. 1. XRD diffractograms of the catalysts: (a) after calcination at 400 °C and 800 °C. (b) After reaction at different conditions of calcination and reaction: (*a*): Ni/Mg-Al, Temp. calc. = 800 °C, Temp. Reac. = 650 °C; (*b*) Ni-Co/Mg-Al, 800 °C, 575 °C; (*c*) Ni-Co/Mg-Al, 400 °C, 550 °C; (*d*) Co/Mg-Al, 400 °C, 675 °C.

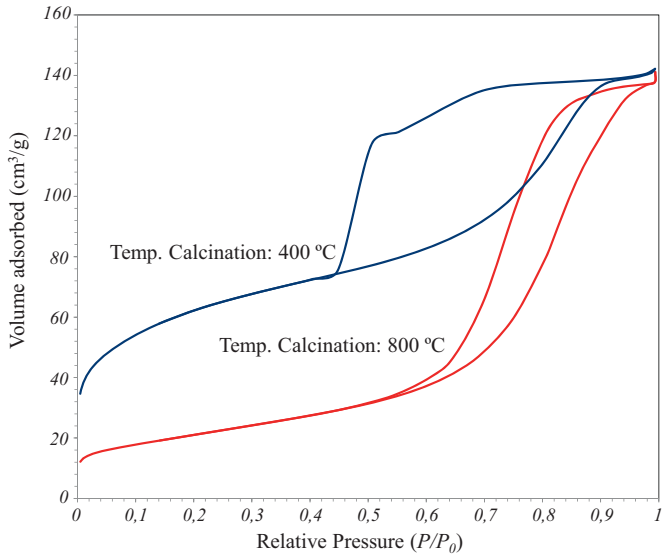

Fig. 2. Nitrogen adsorption and desorption isotherm branches for the Ni-Co/Mg-Al catalyst calcined at 400 °C (blue lines) and 800 °C (red lines). (For interpretation of the references to color in this figure legend, the reader is referred to the web version of the article.)

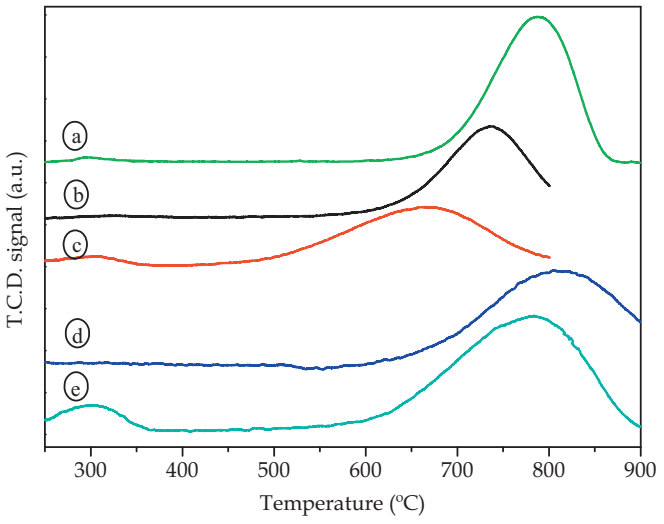

Fig. 3. TPR profiles of the catalysts. (*a*) Ni/Mg-Al; Temp. calc. = 800 °C; (*b*) Ni-Co/Mg-Al, Temp. calc. = 800 °C; (*c*) Ni-Co/Mg-Al; Temp. calc. = 400 °C; (*d*) Co/Mg-Al, Temp. calc. = 800 °C; (*e*) Co/Mg-Al; Temp. calc. = 400 °C.

a hysteresis loop of the type H1 [18], corresponding to materials with well-defined cylindrical-like pore channels distribution [19]. Both samples show mono-modal pore-size distributions with sharp peaks at 5.7 nm (calcined at 400 °C) and 10.6 nm (calcined at 800 °C).

Table 1 shows the results of specific surface area and pore volume measurements for the three catalysts as a function of the calcination and reaction temperatures. In accordance with the XRD results, it can be seen that in all the cases the S_{BET} decreases as the calcination temperature increases. After calcination at high temperature (800 °C), the support structure is partially sinterized and the specific surface area and pore volume related to the micropores, decreases drastically. In the case of the Co/Mg-Al catalyst, part of the metallic nanoparticles of Co can be buried inside the support explaining the lower reactivity showed by these samples. Thus, curve (*d*) on Fig. 1b does not show the presence of CoO nanoparticles. However, in the case of the Ni-Co/Mg-Al catalyst, it can be observed the presence of metallic NiO and CoO, see Fig. 1b, curves (*b*) and (*c*), explaining the high activity of this catalyst at both calcination temperatures.

The TPR profiles for the catalysts calcined and after reaction are shown in Fig. 3. At both calcination temperatures, the samples show a high temperature peak of hydrogen consumption, ranged from 660 to 810 °C. These peaks are assigned to the reduction of Ni^{+2} and/or Co^{+2} species in high interaction with the support. The degree of interaction is determined by the temperature of calcination and therefore is related to the size of the oxide and aluminate phases formed, in accordance with XRD results. In addition, the presence of Co increases the reducibility of Ni^{+2} species as indicate the curves (*a*), (*b*) and (*c*). The lower reducibility of the monometallic catalyst of Co indicate that the Co has higher tendency to form the spinel phase that the Ni. Finally, the low temperature peak in curve (*e*) can be assigned to the reduction of Co^{+3} species formed during the calcination stage.

3.2. Catalytic results. Influence of the reaction temperature

The use of the bimetallic catalyst Ni-Co/Mg-Al aims to combine the best results obtained with the monometallic catalysts. Thus, the Ni/Mg-Al catalyst is very active to decompose methane, and the Co/Mg-Al catalyst is more selective to produce CNT instead other carbonaceous materials.

Table 1
Influence of reaction and calcination temperatures on specific surface area.

Catalyst	Temp. Calc. (°C)	Temp. React. (°C)	S_{BET} (m^2/g)	$S_{micropore}$ (m^2/g)	V_{pore} (cm^3/g)	$V_{micropore}$ (cm^3/g)
Ni/Mg-Al	800	–	178	*	*	*
Co-Mg-Al	400	–	201	59	0.52	0.027
	800	–	74	10	0.54	0.0045
Ni-Co/Mg-Al	400	–	219	49	0.17	0.022
	800	–	76	2.5	0.22	0.0006
Ni-Co/Mg-Al (after reaction)	400	550	129	14	0.68	0.006
	400	625	139	27	0.26	0.012
	800	575	110	0	0.85	0

* Not measured.

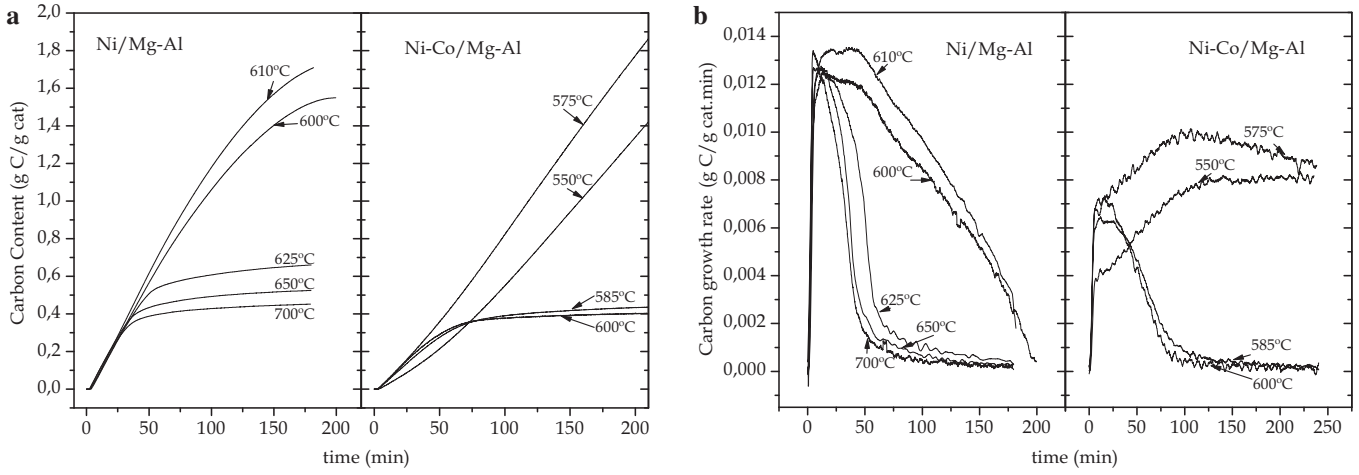

Fig. 4. Influence of reaction temperature on the evolution along time of: (a) carbon content; (b) rate of carbon growth. Catalysts: Ni/Mg-Al and Ni-Co/Mg-Al Temp. calc. = 800 °C.

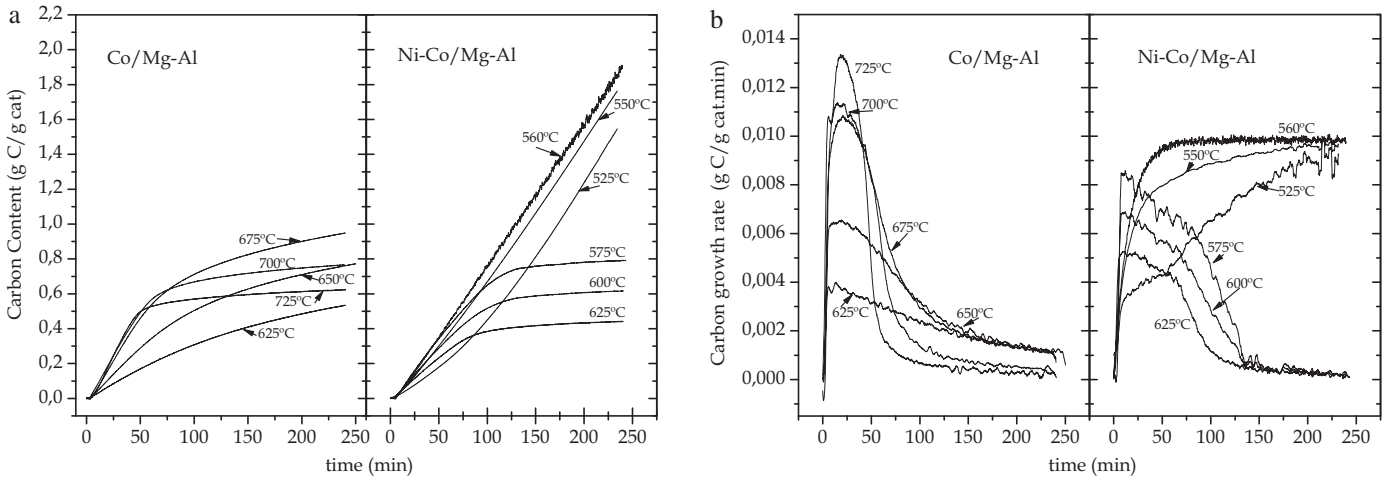

Fig. 5. Influence of reaction temperature on the evolution along time of: (a) carbon content; (b) rate of carbon growth. Catalysts: Co/Mg-Al and Ni-Co/Mg-Al Temp. calc. = 400 °C.

Figs. 4 and 5 show the effects of temperature of reaction over the carbon productivity, expressed as carbon content, and on the reaction rate, expressed as carbon growth rate. Fig. 4a and b corresponds to samples calcined at 800 °C and Fig. 5a and b corresponds to samples calcined at 400 °C. From the data of the reaction rate on Figs. 4b and 5b can be calculated the rate of hydrogen production [8].

From the date presented in Figs. 4 and 5 it can be seen that the ranges of reaction temperatures where the catalysts are active and stable are different for the catalysts studied. In general, all the catalyst presents the same evolution of the activity and stability with the reaction temperature. At low temperature of reaction, the catalysts are active and are more or less stable, depending of their composition. As the temperature increases, the rate of CNT formation increase, but also the deactivation of the catalyst is more marked. Thus, for all the catalyst there is one temperature at which a maximum productivity is attained. This maximum depends on the catalyst composition and on the temperature of calcination. Thus, the maximum productivity is reached at 560 °C and 575 °C for the bimetallic catalyst calcined at 400 and 800 °C respectively. For the monometallic catalysts the maximum are achieved at 610 °C (Ni/Mg-Al, calcined at 800 °C) and 675 °C (Co/Mg-Al, calcined at 400 °C). These values represent the transition temperatures, above which the deactivation of the catalyst becomes quite pronounced, and the carbon production stops in a few minutes.

Ni/Mg-Al is the catalyst that presents the broader interval of reaction temperatures in where the catalysts studied are active. However, at all the temperatures studied shows a loss of activity, which is very pronounced above 610 °C. This effect is clearly showed in Fig. 4b. In all the cases, the reaction rate rapidly increases at the beginning of the reaction, attaining a maximum value. From this point, and as a consequence of the activity decay, the reaction rate decreases until that a residual value is reached. In the case of Ni/Mg-Al, at temperatures below 610 °C the deactivation rate is low. The presence of these maximums is consequence of the mechanism of CNT formation as will be discussed in the next paragraph.

The Co/Mg-Al catalyst shows deactivation at all the temperatures studied (see Fig. 5b), although the maximum rate attained at 725 °C, after 5 min of reaction, is quite similar to the maximum values obtained with the Ni/Mg-Al catalyst (Fig. 4a). As can be seen in Fig. 5b, the value of this maximum increases with the reaction temperature, but also augments the deactivation rate.

The bimetallic catalyst presents a remarkable stability at low reaction temperatures (Figs. 4 and 5). This fact is the cause of the high productivity reached at the end of the reaction, in spite of the maximum values of the reaction rate showed by this catalyst, at both temperatures of calcination, is lower that of the monometallic catalysts (see Figs. 4b and 5b). However, at temperatures above the transition temperature, this catalyst also suffers deactivation. Noticeably, there is a window of operating temperatures in which is possible to produce hydrogen and nanocarbonaceous materials at constant rate, i.e. in steady conditions. This window can be modulated by the catalyst composition, the feed composition (e.g. ratio hydrogen/methane) and the spatial velocity used in the reactor. Hence, the greater hydrogen productivity attained with the bimetallic catalyst operating at stable conditions, i.e. at low reaction temperatures, is ca. 0.210 g H_2/g cat. h.

3.3. Kinetic modeling

In this section we present the results obtained from the application of the *Phenomenological Kinetic Model* [14–16] to the experimental results obtained with the Ni-Co/Mg-Al catalyst. In this study, the application of this model allows us to improve the knowledge of the influence of the operating conditions on each of the individual stages involved in the CNT formation. Briefly, the model considers the following stages:

(i) *Carburization–nucleation*: After methane decomposition, the remaining carbon atoms react with the metallic nanoparticles at the surface forming a shell of metastable carbide that, at the reaction conditions used, decomposes leaving carbon atoms at the metallic subsurface [20]. After this decomposition–segregation step, the carbon atoms are introduced inside the metal particles [20], determining the value of the carbon concentration at the carbide-metallic nanoparticle interphase (C_S). The rate of this stage is given by [16]:

$$r_S = \frac{dC_S}{dt} = \psi_S(1 + K_S C_S)(C_{S_m} - C_S) \quad (1)$$

In this equation C_S is the concentration of surface carbide and has units of (g C/g cat.). ψ_S represents the intrinsic *kinetic function of carburization*. C_{Sm} represents the maximum surface carbide concentration attainable on the surface of metallic particles at the side gas phase. The parameter K_S represents the contribution of the autocatalytic effect on the carburization kinetics. It assumed that the carburization stage occurs at the beginning of the reaction, before that the catalyst deactivation is appreciable. In fact, at this initial time there is a strong increase of the reaction rate (see Figs. 4b and 5b).

(ii) *Diffusion–precipitation*: The rate of the diffusion-precipitation process determines the intrinsic rate of formation of carbon nanotubes (r_C). In the case of methane decomposition, the rates of methane conversion, CNT formation, and hydrogen production are stoichiometrically related by [8]: $(-r_{CH_4})_t = (r_{H_2})_t/2 = (r_C)_t$. If we assume unidirectional diffusion, this initial reaction rate can be expressed in terms of a classical diffusion equation as [15,16]:

$$(r_C)_0 = \left.\frac{dm_C}{dt}\right|_{t=0} = k_C(C_S - C_F) \cong k_C C_S \quad (2)$$

The term k_C is the effective coefficient of carbon transport along the metallic nanoparticles, and have dimension of time^{-1}. It has also been assumed that the value of C_F (the carbon concentration in the metallic particles at the support side) is very low compared to the value of C_S.

(iii) *Catalyst deactivation*: Simultaneously to CNT growth, formation of encapsulating coke usually occurs, which can deactivate the catalyst over time. The decrease of the reaction rate can be expressed in terms of catalyst activity, a, as follows [14,16]:

$$(r_C)_t = \left.\frac{dm_C}{dt}\right|_{t>0} = (r_C)_0 a = k_C C_S a \Leftrightarrow a = (r_C)_t/(r_C)_0 \quad (3)$$

In the above equation, the terms a and $(r_C)_0$ vary along reaction time, and represent the remainder catalyst activity and the initial CNT growth rate, respectively. Therefore, the term $(r_C)_0$ is the reaction rate of the fresh catalysts, without deactivation. If the formation of encapsulating carbon is partially reversible, i.e. there is partial gasification of the carbon by the H_2 present in the gas phase, the net deactivation rate can be expressed as [16,21]:

$$r_d = -\frac{da}{dt} = \psi_d a^d - \psi_r(a^{d_m} - a) \quad (4)$$

The terms ψ_d and ψ_r are respectively the "*deactivation and regeneration kinetic functions*", and both also depend on the operating conditions. In addition, the values of the kinetic orders d and d_m are calculated considering the number of sites involved in the controlling step of the main reaction (m), and of the deactivation reaction (h) as follows [21] $d = (m + h - 1)/m$ and $d_m = (m - 1)/m$. For the case of methane decomposition it is assumed that $m = 2$ and $h = 1$ and therefore $d = 1$ and $d_m = 1/2$ [8,14].

A complete description of all these stages has been previously presented [15,16]. The numerical solution of the above set of ordinary differential equations 1, 3 and 4 allows the calculation of the evolution along time of the mass of CNTs formed (m_C), the rate of CNT growth, (r_C), the concentration of surface carbide, (C_S) and of the catalyst activity (a). The kinetic parameters displayed in Tables 2 and 3 were calculated by non-linear regression of the experimental values of m_C and r_C presented in Figs. 4 and 5. As indicate the high values of r^2 (coefficient of determination), and the low values of standard error of the parameters, the fitting of the model to the data is very good in all the cases.

These kinetic parameters obtained also indicate the presence of a transition temperature above which the deactivation of catalyst prevails. Thus, for the bimetallic catalyst calcined at 400 and 800 °C, these temperatures are 570 °C and 580 °C respectively. The existence of this critical temperature has been also observed on similar catalysts [9–11,14] and it is a consequence of the competition between several parallel processes: (i) the carbon diffusion through the particles that finally form the carbon nanotubes, and the reversible formation of encapsulating carbon, responsible for the deactivation. This encapsulating carbon can be partially gasified by the hydrogen present in the reaction atmosphere cleaning the surface of the metallic nanoparticles and therefore maintaining their activity [14]. The different activation energies of these steps explain the great influence of the reaction temperature over

Table 2
Influence of reaction temperature on the kinetic parameters. Temperature of calcination: 400 °C.

Reaction Temp. (°C)	$j_{C_0} \times 10^3$ (g C/g cat. min)	$\psi_S \times 10^2$ (min^{-1})	$\psi_d \times 10^3$ (min^{-1})	ψ_r (min^{-1})	r^2 (CD)
525	6.64 ± 0.357	6.14 ± 0.312	0	2.47 ± 0.096	0.9785862
550	7.66 ± 0.130	10.2 ± 0.755	0	5.40 ± 0.397	0.9983165
560	8.68 ± 0.228	14.2 ± 0.238	0	1.13 ± 0.246	0.9999895
575	18.1 ± 0.848	0.521 ± 0.045	49.70 ± 2.07	17.1 ± 0.650	0.9999707
600	14.3 ± 0.645	0.715 ± 0.056	39.85 ± 1.78	17.9 ± 0.653	0.9999973
625	10.3 ± 0.36	1.00 ± 0.24	41.86 ± 2.04	19.5 ± 0.477	0.9984231

Table 3
Influence of reaction temperature on the kinetic parameters. Temperature of calcination: 800 °C.

Reaction Temp. (°C)	$j_{C_0} \times 10^3$ (g C/g cat. min)	$\psi_S \times 10^2$ (min^{-1})	$\psi_d \times 10^2$ (min^{-1})	$\psi_r \times 10^3$ (min^{-1})	r^2 (CD)
550	7.92 ± 0.53	3.25 ± 0.78	0	0	0.9996022
575	9.58 ± 0.49	8.01 ± 0.26	0.015 ± 0.004	0	0.9999928
585	87.1 ± 2.1	1.12 ± 0.03	4.56 ± 0.32	2.10 ± 0.324	0.9999996
600	353.5 ± 3.3	0.34 ± 0.04	5.54 ± 0.63	1.17 ± 0.21	0.9999995

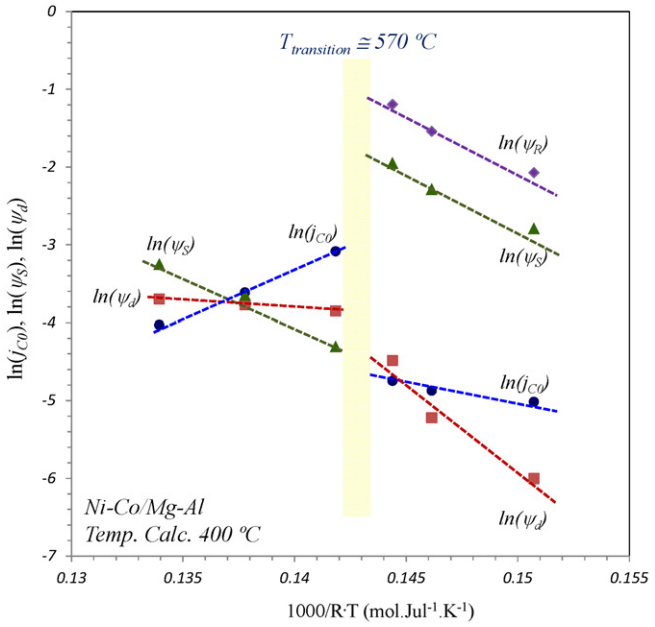

Fig. 6. Arrhenius plot of the kinetic parameters corresponding to the Ni-Co/Mg-Al catalyst calcined at 400 °C.

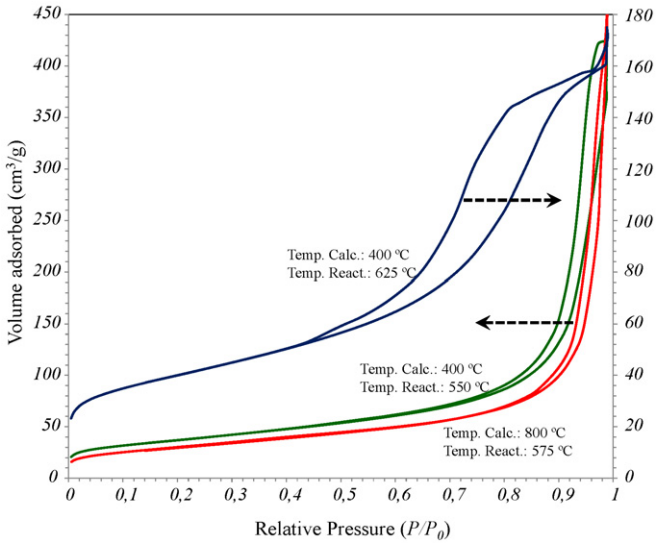

Fig. 7. Nitrogen adsorption and desorption isotherm branches for the Ni-Co/Mg-Al catalyst after reaction.

the net rate of carbon accumulation on the catalyst observed in Figs. 4 and 5. The temperature of transition is strongly dependent on the catalyst composition, because the effective coefficient of carbon diffusion on the metallic nanoparticles depends on several factors like the size distribution, that gives the average path of diffusion; the chemical composition, that limits the carbon diffusivity, and the type of support, that controls the degree of metal-support interaction, and therefore the particle size distribution and morphology, and therefore the CNT's diameter.

In Fig. 6 is presented the Arrhenius plot for the data corresponding to the bimetallic catalyst calcined at 400 °C. It can be seen clearly the noticeable change of the activation energies and of the pre-exponential factors of the kinetic parameters. The more important changes in the activation energies are suffered by the *deactivation function of regeneration*, ψ_d, and by the parameter j_{C_0}. This term represents the maximum allowable carbon flux (g C/g cat. min) that can be obtained through the metallic nanoparticles of the catalysts, and is given by: $j_{C_0} = k_C C_{S_m}$. Therefore, the change in the apparent activation energy of this parameter is due to the change in the effective coefficient of carbon transport, k_C. At high reaction temperatures, both parameters, ψ_d and j_{C_0}, show a reduction of the activation energy. These values are about 170 (low temp. zone) and 20 (high temp. zone) KJ μl/mol for ψ_d and 30 (low temp. zone) and −90 (high temp. zone) KJ μl/mol for j_{C_0}. The values are poorly estimated due to the low number of experiences at each zone, and the last negative value is due to this fact. However, the tendency is clear, indicating a change in the controlling step of the carbon formation over the catalyst, dominating the formation of encapsulating carbon at reaction temperatures. As regards, the parameter ψ_S, there is not an appreciable change of the activation energy, from 95 to 104 KJ μl/mol, but the decrease of the pre-exponential factor is notorious due to the decrease of the available surface of the metallic nanoparticles, after the formation of encapsulating carbon. The trends observed at 800 °C are very similar (see Table 3).

3.4. Characterization of the nanocarbonaceous materials after reaction

The carbon obtained after reaction under different operating conditions was characterized by TEM, TPO, XRD and N_2 adsorption.

Fig. 7 shows the N_2 adsorption/desorption isotherms for the Ni-Co/Mg-Al catalyst after reaction. These isotherms correspond to isotherms type IV, but the hysteresis loops of the samples at low reaction temperature (550 °C and 575 °C) are of the type H3 [18]. This type of hysteresis do not seems to have any adsorp-

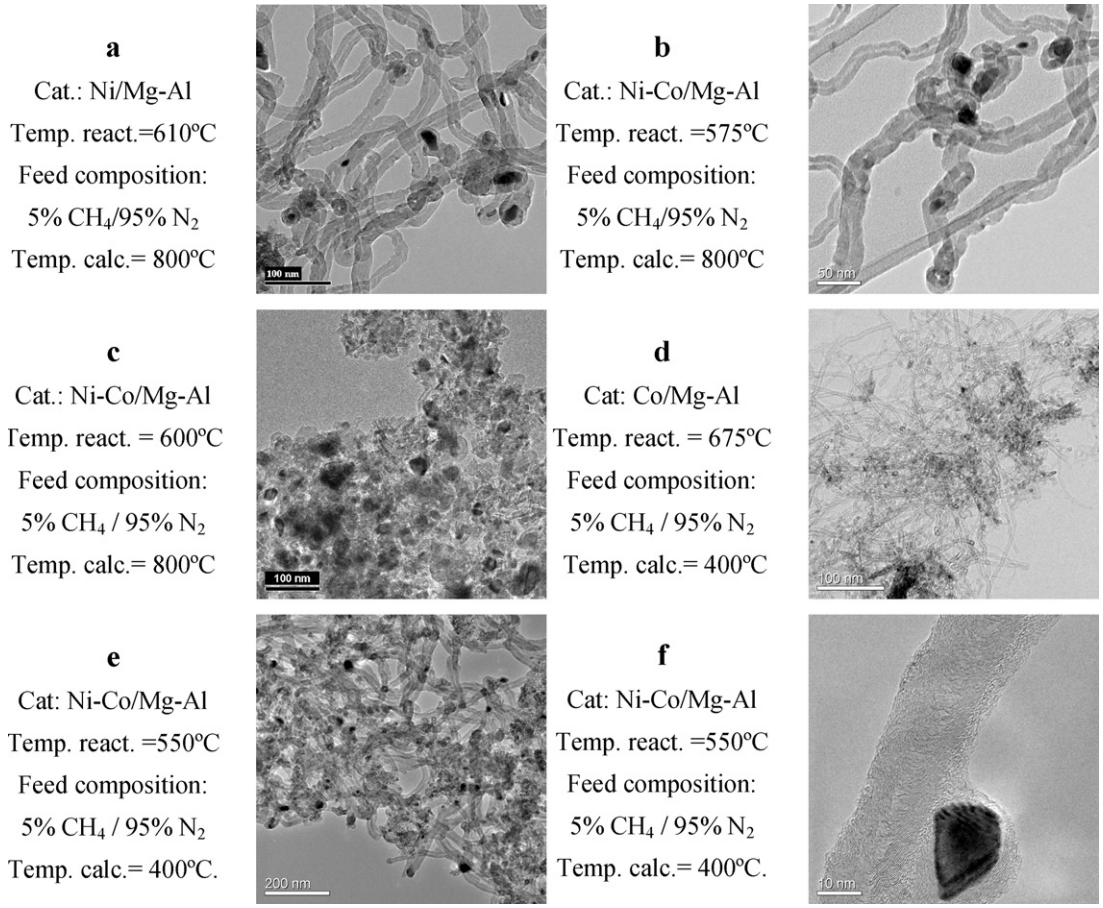

Fig. 8. TEM images of the catalysts after reaction at different operating conditions.

tion limit at high values of the relative pressure, P/P_0, and are associated to materials containing non-rigid aggregates of plate-like particles giving rise to slit-shaped pores [19]. This behavior is consequence of the presence of CNTs and other carbonaceous materials inside the pore structure. The data in Table 1, corresponding to the specific surface and pore volume of the micropores, are in accordance with this hypothesis. Thus, the sample calcined 400 °C, after reaction at 550 °C contains a very high carbon content (see Fig. 4a) and present a micropore volume of 0.006 cm^3/g, while before reaction, this volume was 0.022 cm^3/g. However, if the reaction is carried out at 625 °C, the carbon productivity is quite lower due to the catalyst deactivation, and in consequence the decrease observed in the micropore volume is lower (0.012 cm^3/g, see Table 1). In the case of the sample calcined at 800 °C, the micropore volume before reaction was very low (0.0006 cm^3/g), and therefore after reaction this value is negligible. On the other hand, the sample calcined at 400 °C, after reaction at 625 °C shows a hysteresis loop of the type H1 [18], although before reaction this sample showed an hysteresis loop of type H3. This change, as is indicated by comparison of XRD results in Fig. 1a and b (curve (*c*)), is due to the thermal modification of the catalyst structure produced during the reaction at 625 °C. Then, the final structure is similar that that obtained after calcination at higher temperature, see Fig. 1b, curve (*b*). This fact also explains the decrease of the BET surface area obtained after reaction in spite of carbon nanotubes formation (see Table 1). On the contrary, in the case of the sample calcined at 800 °C, there is a notorious increase of the BET surface area, which is due to the presence of the carbon nanotubes. Given that during the reaction there is not any additional modification of the structure, the growth of the nanocarbonaceous materials over de surface produces the observed increase of the surface area.

In Fig. 8, are presented some TEM micrographs corresponding to the three catalysts after several reaction conditions. The carbon nanotubes generated with the Ni-Co/Mg-Al and Ni/Mg-Al catalysts, calcined at 800 °C and after the reaction at their optimum temperature (575 and 610 °C respectively), show similar features. The morphology of these carbonaceous materials corresponds to multi-walled carbon nanotubes (MWNT), with an average diameter of ca. 20 nm (see Fig. 8a and b). Therefore, the addition of Co to the catalyst Ni/Mg-Al improves the stability of the catalyst without modifying significantly the selectivity to the formation of MWNT.

A small proportion of metallic agglomerations forming particles of large size can also be observed owing to the sinterization caused by the high calcination temperature used in this case (800 °C).

Fig. 8c corresponds to a micrograph of the bimetallic catalyst after calcination at 800 °C and reaction at 600 °C, i.e. above their transition temperature and therefore under severe deactivation (Fig. 4b), in agreement with the large quantity of amorphous encapsulating carbon observed in this case. The presence of big metallic nanoparticle observed in this sample is due to the catalyst sinterization.

De Chen et al. [22] have shown that both, the CNT formation rate and the encapsulating carbon formation rate, greatly depends on the size of the metallic crystallites formed in the catalyst after calcination and reduction stages. Thus, an optimum nanoparticle size appearing from which the reaction rate dimin-

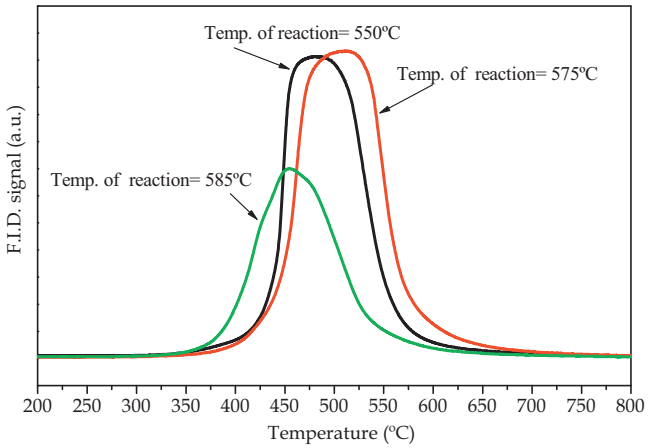

Fig. 9. TPO results of the Ni-Co/Mg-Al catalyst calcined at 800 °C, after reaction at 550, 575 and 585 °C respectively.

ishes. The optimum size changes with the catalyst composition. This fact explains why the range of operating temperatures, and also the transition temperature, is different for each catalyst. Consequently, the formation of a major proportion of encapsulating carbon is favored on large sized metallic particles, due to the difficulty of carbon diffusion through big particles. In summary, the type and quantity of nanocarbonaceous materials formed during the reaction depends to a great extent on the reaction temperature.

Fig. 8d shows the carbon obtained with the Co/Mg-Al catalyst calcined at 400 °C and after reaction at the optimum temperature, 675 °C (see Fig. 5a). It can be observed that the low calcination temperature produces a solid of low crystallinity, which contains particles of very small size. In consequence, the carbon nanotubes produced also have low diameters (~4 nm).

After reaction at 550 °C with the Ni-Co/Mg-Al catalyst calcined at 400 °C, the images exhibit a homogeneous sample, made up of carbon nanotubes and a small proportion of amorphous carbon (Fig. 8e). However, it should be emphasized that the morphology of the carbon nanotubes formed has changed with respect to the catalyst calcined at 800 °C and to the base catalyst Co/Mg-Al. In this case, these carbonaceous materials are herringbone carbon nanofibres, with diameters of ca. 20 nm and graphene layers oriented obliquely to the filament axis. Besides, this image reveals a metallic particle encapsulated by carbon and, therefore, deactivated.

In Fig. 9, are presented the TPO results of the samples after reaction at 550, 575 and 585 °C for the bimetallic catalyst calcined at 800 °C. These results indicate that the carbon formed at low temperature, i.e. below the transition value, is mainly of graphitic nature and is forming CNTs, in agreement with TEM results. However, the carbon formed at 585 °C contains amorphous, or less graphitic, encapsulating carbon that is more easily burned. The areas of the TPO peaks of the samples after reaction at 550 and 575 °C are almost the same given of the similar carbon productivity of the catalyst at these two temperatures (see Fig. 4a). However, after reaction at 585 °C, the peak area is much lower owing to the lower activity of the catalyst (see Fig. 4a). These facts are in agreement with TEM observations, which show that when the catalyst does not suffer deactivation, the carbon obtained is mainly formed by carbon nanotubes (Fig. 8e). However, if deactivation occurs, the carbon mainly corresponds to amorphous carbon (Fig. 8f).

4. Conclusions

The catalyst activity, selectivity and resistance to deactivation during the production of hydrogen and carbon nanotubes by catalytic decomposition of methane depend on the catalyst composition, and on the conditions of calcination and reaction. The ranges of reaction temperatures where the catalysts are active and stable are mainly determined by the catalyst composition. At low temperature of reaction, the catalysts have higher stability. As the temperature increases the rate of CNT formation increase, but also the deactivation of the catalyst is more marked, becoming the dominant effect.

The bimetallic Ni-Co/Mg-Al catalyst is stable at reaction temperatures below 580 °C, the transition temperature. Therefore, it is possible to produce hydrogen and nanocarbonaceous materials in steady conditions, which is a critical factor for the industrial development of this process. This transition temperature depends on the catalyst composition, the feed composition (e.g. ratio hydrogen/methane) and the spatial velocity used in the reactor. The greater hydrogen productivity attained with the bimetallic catalyst operating at stable conditions is ca. 0.210 g H_2/g cat. h. The temperature of calcination does not affect the stability of the bimetallic catalyst operating at low temperatures of reaction.

The change of the kinetic behavior of the catalysts at the transition temperature is a consequence of the competence between the surface carbide formation, necessary to the nucleation and growth of the CNTs, and the formation of encapsulating carbon, which deactivates the catalyst. The value of this transition temperature is determined by the energies of activation of both steps. Finally, at low operating temperatures the morphology of the carbonaceous materials, corresponds to MWNT or herringbone carbon nanofibres, with average diameter of ca. 20 nm. At high reaction temperature the carbonaceous material formed contains substantial amounts of amorphous carbon.

Acknowledgements

The authors acknowledge financial support from MICINN (Spain)-FEDER, Projects CTQ 2007-62545/PPQ, and CTQ2010-16132, and the Regional Government of Aragón, Departamento de Ciencia, Tecnología y Universidad, Project CTP P02/08.

References

[1] M.S. Dresselhaus, G. Dresselhaus, Ph. Avouris (Eds.), Carbon Nanotubes: Synthesis, Structure, Properties and Applications, Springer-Verlag, Berlin, 2001.
[2] K.P. De Jong, J.W. Geus, Catal. Rev. Sci. Eng. 42 (2000) 481.
[3] P. Serp, M. Corrias, P. Kalk, Appl. Catal. A 253 (2003) 337.
[4] C.E. Baddour, C. Briens, Int. J. Chem. React. Eng. 3 (2005) R3, http://www.bepress.com/ijcre/vol3/R3.
[5] S.B. Sinnott, R. Andrews, D. Qian, A.M. Rao, Z. Mao, E.C. Dickey, F. Derbyshire, Chem. Phys. Lett. 315 (1999) 25.
[6] J.N. Armor, Appl. Catal. A: Gen. 176 (1999) 159.
[7] A.M. Amin, E. Croiset, W. Epling, Int. J. Hydrogen Energy 36 (2011) 2904.
[8] J.I. Villacampa, C. Royo, E. Romeo, J.A. Montoya, P. Del Angel, A. Monzón, Appl. Catal. A: Gen. 252 (2003) 363.
[9] A. Monzón, N. Latorre, T. Ubieto, C. Royo, E. Romeo, J.I. Villacampa, L. Dussault, J.C. Dupin, C. Guimon, M. Montioux, Catal. Today 116 (2006) 264.
[10] M. Monthioux, L. Noé, L. Dussault, J.C. Dupin, N. Latorre, T. Ubieto, E. Romeo, C. Royo, A. Monzón, C. Guimon, J. Mater. Chem. 17 (2007) 4611.
[11] N. Latorre, J.I. Villacampa, T. Ubieto, E. Romeo, C. Royo, A. Borgna, A. Monzón, Topics Catal. 51 (2008) 158.
[12] N. Latorre, T. Ubieto, J.I. Villacampa, C. Royo, E. Romeo, A. Monzón, Producción de hidrógeno y nanotubos de carbono sobre catalizadores de Co-Mg-Al por descomposición catalítica de metano, in: Actas XXI Simposio Iberoamericano de Catálisis, Málaga, España, 2008.
[13] P. Benito, M. Herrero, F.M. Labajos, V. Rives, C. Royo, N. Latorre, A. Monzon, Chem. Eng. J. 149 (2009) 455.
[14] N. Latorre, E. Romeo, J.I. Villacampa, F. Cazaña, C. Royo, A. Monzón, Catal. Today 154 (2010) 217.
[15] A. Monzon, G. Lolli, S. Cosma, M. Sayed-Ali, D.E. Resasco, J. Nanosci. Nanotechnol. 8 (2008) 6141.
[16] N. Latorre, E. Romeo, F. Cazaña, T. Ubieto, C. Royo, J.I. Villacampa, A. Monzón, J. Phys. Chem. C 114 (2010) 4773.
[17] E. Romeo, C. Royo, A. Monzón, R. Trujillano, F.M. Labajos, V. Rives, Stud. Surf. Sci. Catal. 130 (2000) 2099.

[18] K.S.W. Sing, D.H. Everett, R.A.W. Haul, L. Moscou, R.A. Pierotti, J. Rouquerol, T. Siemieniewska, Pure Appl. Chem. 57 (1985) 603.
[19] S. Lowell, J. Shields, M.A. Thomas, M. Thommes, Characterization of Porous Solids and Powders: Surface Area Pore Size and Density, Springer, Dordrecht, The Netherlands, 2006.
[20] I. Alstrup, J. Catal. 109 (1988) 241.
[21] J.C. Rodriguez, J.A. Peña, A. Monzón, R. Hughes, K. Li, Chem. Eng. J. 58 (1995) 7.
[22] D. Chen, K.O. Christensen, E. Ochoa-Fernández, Z. Yu, B. Tøtdal, N. Latorre, A. Monzón, A. Holmen, J. Catal. 229 (2005) 82.